Available online at www.sciencedirect.com
SCIENCE DIRECT®
Journal of the European Ceramic Society 25 (2005) 1275–1283
www.elsevier.com/locate/jeurceramsoc

Environmental effects on ultra-high temperature creep behavior of directionally solidified oxide eutectic ceramics

Yoshihisa Harada [a,*], Takayuki Suzuki [a], Kazumi Hirano [a], Narihito Nakagawa [b], Yoshiharu Waku [c]

[a] *Advanced Manufacturing Research Institute, National Institute of Advanced Industrial Science and Technology (AIST), Tsukuba, Ibaraki 305-8564, Japan*
[b] *Ube Research Laboratory, Corporate Research and Development, UBE Industries, Ltd., Ube, Yamaguchi 755-8633, Japan*
[c] *Engineering Research Association for High Performance Gas Turbine, Ube, Yamaguchi 755-0001, Japan*

Available online 9 February 2005

Abstract

Experimental studies were undertaken to assess the environmental effects on ultra-high temperature tensile creep behavior of directionally solidified $Al_2O_3/Y_3Al_5O_{12}$(YAG) and $Al_2O_3/GdAlO_3$(GAP) eutectic ceramics. Tensile creep deformation tests conducted under constant stress ranging 100–200 MPa at temperature range of 1673–1873 K at different environmental conditions consisting of air and at different water vapor pressure, p_{H_2O}, up to 0.6 MPa. These eutectic ceramics exhibited a stress exponent of about 4.9–11.6, indicative of tensile creep behavior characteristic of dislocation mechanism. The apparent activation energy for creep deformation was 737–984 kJ/mol of Al_2O_3/YAG and 957 kJ/mol of Al_2O_3/GAP in air, while it was 529–645 kJ/mol of Al_2O_3/YAG and 611 kJ/mol of Al_2O_3/GAP at p_{H_2O} = 0.06 MPa and 570–620 kJ/mol of Al_2O_3/YAG at p_{H_2O} = 0.6 MPa. The presence of moisture accelerated the creep rate by about 1.4–4 orders of magnitude for p_{H_2O} = 0.06 MPa, about five orders of magnitude for p_{H_2O} = 0.4 MPa and about 5–7 orders of magnitude for p_{H_2O} = 0.6 MPa as compared with that in air at 1773 K. Results of this study and reasonable estimates in changes of the water vapor pressure indicated accelerated creep behavior by the presence of moisture.

Keywords: Direcionally solidification; Creep; Al_2O_3

1. Introduction

Directionally solidified oxide eutectic ceramics, named melt growth composites (MGCs), have been developed and studied in bulk processed materials; some MGCs are $Al_2O_3/Y_3Al_5O_{12}$(YAG), $Al_2O_3/GdAlO_3$(GAP), $Al_2O_3/Er_3Al_3O_{12}$(EAG) binary systems and Al_2O_3/EAG/ZrO_2 ternary system.[1–6] The Al_2O_3/YAG system has a new microstructure in which single-crystals Al_2O_3 and YAG consist of fine lamellar and three-dimensional networking structures. This material is thermally stable even at the high temperature of 1973 K for 1000 h in air. It has an excellent strength over 1773 K and a good productivity of complex structural components compared to conventional sintered engineering ceramics. Such a material is potential candidate for ultra-high temperature structural materials in power generation and aerospace industries. However, in such applications, a considerable amount of water vapor can be encountered in the service environment. In addition, it involves synergistic interactions between corrosion and deformation processes. In metals and alloys, hydrogen impurities in moist environments are fast diffusing species that can be trapped by dislocations and grain boundaries.[7] This leads to the hydrogen embrittlement. In metal oxides, hydrogen impurities generally diffuse much more slowly than in metals,[8] however, lead to pronounced reductions in the strength.[9–11]

It is well established that slow crack growth in alumina and sapphire is promoted by moisture in air,[12,13] thus decreasing fracture strength in atmospheric environments. Much less is known about reductions of strengths with interstitial hydrogen defects. Heuer et al.[14] reported that polycrystalline

* Corresponding author. Tel.: +81 29 861 7169; fax: +81 29 861 7853.
E-mail address: harada.y@aist.go.jp (Y. Harada).

0955-2219/$ – see front matter © 2005 Elsevier Ltd. All rights reserved.
doi:10.1016/j.jeurceramsoc.2005.01.028

Al_2O_3 subjects to high pressure (1400 MPa) water vapor conditions, similar to those used to weaken quartz,[15] is found to deform at stresses far lower than those measured in dry tests at 1473 K. A recent study of hydrothermally grown sapphire suggests that "wet" α-Al_2O_3 crystals exhibit enhanced dislocation processes.[11] Such extensive research on mechanical properties at high-temperatures has been conducted over the past decades, but little attention has been given to effects of several environments, especially moist environments.[16,17]

We are the first to construct a material testing system that simulates severe environments such as ultra-high temperature and high-pressurized water vapor.[16] The equipment conducts mechanical tests at ultra-high temperature up to 1973 K, and high pressures to 0.98 MPa in air, moist, and gas environments. We have used it to study tensile creep behavior of Al_2O_3/YAG system at 1773–1873 K.[16,17] This study used tensile creep test at ultra-high temperature in air and at different high-pressurized water vapor to evaluate environmental effects on creep deformation in Al_2O_3/YAG and Al_2O_3/GAP systems.

2. Experimental procedures

High-purity commercial α-Al_2O_3 powders (AKP-30, 99.99%; Sumitomo Chemical Co. Ltd.), Y_2O_3 (Y_2O_3-SU, 99.999%; Shin-etsu Chemical Co., Ltd.) and Gd_2O_3 (Gd_2O_3-RU, 99.999%; Shin-etsu Chemical Co., Ltd.) were used for starting materials. These powders were ball-milled in ethanol with 82 mol.% Al_2O_3–18 mol.% Y_2O_3 or 78 mol.% Al_2O_3–22 mol.% Gd_2O_3 to form a material with 50 vol.% of each Al_2O_3 and YAG (GAP) phase. After removing ethanol and drying the slurry with a rotary evaporator, these powders were pre-melted to yield an ingot that was subsequently placed in a molybdenum crucible. It was fabricated by unidirectional solidification in a crucible using a Bridgman-type apparatus (Japan Ultra-high Temperature Materials Research Center, Ube, Japan) at a melting temperature of 2173 K, lowering the crucible at 1.39×10^{-6} m/s.[1–3] Cylindrical tensile creep specimens were machined with their axis parallel to the direction of solidification. The specimen geometry was approximately 2.5 mm in gage-diameter, with a 10 mm gage-length and 65 mm long overall (see Fig. 1). All specimens were heated at 1873 K for 1 h in air after machining.

Constant-load tensile creep tests were conducted in several environments using an ultra-high temperature materials testing system developed for simulating severe environments (as described in Ref. [16]). This apparatus was configured with severe environmental simulator generating an ultra-high temperature over 1773 K and high pressure range up to 0.98 MPa using a slow strain rate testing machine as a basic unit. The testing machine was controlled with the crosshead speed range of 0.0001–0.1 mm/min and maximum load up to 20 kN using a closed loop servomotor. Test temperature was measured by two sets of B-type (Pt–Rh) thermocouples located near the specimen gage length. Temperature was maintained

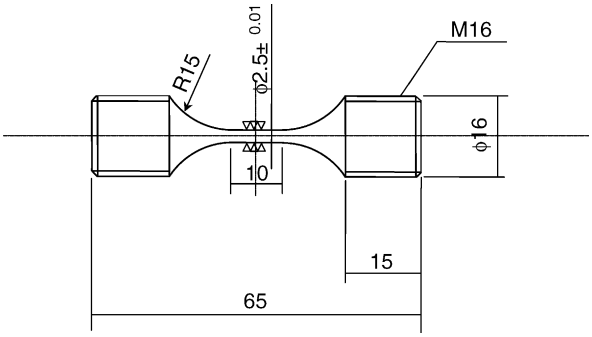

Fig. 1. Geometry of the tensile creep specimen.

within ±1 K of the set point throughout each test after a 2 h soak at the test temperature (after a 5 h soak in the case of a moist environment). Jigs made of Al_2O_3/YAG system applied the load to the specimen.

Test environments in the present investigation considered of dry synthetic air (relative humidity: 30%) and high-pressurized water vapor up to $p_{H_2O} = 0.6$ MPa. For the test in a moist environment, the slow flowing H_2O (1.0 mL/min) was injected into a water vapor stream above the condensation point and heated to the exposure temperature in the interior of an alumina chamber. A pre-load of 5 MPa was applied to avoid any alignment changes during heating. Constant stress on the specimen was controlled to within 1 MPa. Specimen displacement was measured through a linear variable differential transducer with a resolution of 0.5 μm connected to an extensometer, which was attached to load train. The displacement and time were continuously monitored during creep tests.

Hydroxyl concentrations of several samples were determined using Fourier transform infrared (FTIR) spectrometer (2000; Perkin Elmer, Inc.). Experimental specimens were cut with their axis perpendicular to the direction of solidification in the gage section. Central areas of these samples were ground and polished on both sides to thicknesses of 0.5–2 mm. The FTIR spectra were taken in 2000–4000 cm^{-1} range at room temperature in a chamber of the spectrometer with IR radiation passing through a large aperture (2 mm diameter) centered on the specimen surface. After making a background correction using a third-order polynomial fit to the background absorbance, hydroxyl concentration was calculated from infrared spectra by integrating across the hydroxyl bands. Specifically, the hydroxyl concentration was determined from the following relationship based on Beer–Lambert law between total integrated molar absorbance and wave number reported by Kronenberg et al.[18]:

$$[OH] = 0.641\Delta, \quad (1)$$

where [OH] is hydroxyl concentration in ppm (number of OH per 10^6 Al ions) and Δ is integrated absorbance (in 1 cm^{-2}).

Microstructural observation was performed by scanning electron microscopy (JEOL6400Fs; JEOL, Ltd.) and transmission electron microscopy (JEOL200CX; JEOL, Ltd.).

TEM foils were prepared by dimple polishing on one side and ion beam thinning of both sides. Density of creep specimens was measured by Archimedes' method in ethanol (99.8%) before and after creep testing. Specimens were cleaned in ethanol and dried prior to measurement. Density measurements of specimens in the gage-section indicated density of $4.30 \pm 0.01\,g/cm^3$ for the Al_2O_3/YAG system and $5.71 \pm 0.02\,g/cm^3$ for the Al_2O_3/GAP system indicated no significant density changes after creep testing.

3. Results

3.1. Microstructure

Fig. 2 shows scanning electron micrograph of the cross-section parallel to the solidified direction of Al_2O_3/YAG and Al_2O_3/GAP systems. In Fig. 2(a), the bright area is the YAG phase; the dark area is the Al_2O_3 phase. The as-received homogeneous microstructure shows a fine lamellar structure consisting of 1–20 μm in width of each phase, and a three-dimensional network structure containing a single-crystal YAG with a garnet structure distributed in a single-crystal Al_2O_3 with a corundum structure. Fig. 2(b) shows a SEM image of the Al_2O_3/GAP system. The bright area is the GAP phase; the dark area is the Al_2O_3 phase. The Al_2O_3/GAP system has a single-crystal Al_2O_3 and a single-crystal GAP with a perovskite structure consisting of 1–10 μm in width of each phase. The microstructure has a finer structure than that for the Al_2O_3/YAG system. In both systems no pores or no colonies is observed at as-received conditions.

Fig. 3 shows SEM images of the fracture surface for Al_2O_3/YAG and Al_2O_3/GAP systems that has been subjected to creep at 1773 K and a water vapor pressure, p_{H_2O}, of 0.06 MPa. In Fig. 3(a) and (c), both systems fractures are initiated at internal flaws (marked with a circle) that may be attributable to shrinkage voids or micropores. These SEM images show that the brittle fracture morphology of quasi-cleavage and limited ductile deformation are observed (see Fig. 3(b) and (d)). Fundamentally, there was no difference in the creep failure mechanism for air and moist environments, which is assigned to the local microstructure.

3.2. Creep behavior in air

Fig. 4(a) shows stress dependence of minimum creep rate for Al_2O_3/YAG and Al_2O_3/GAP systems at 1673–1873 K in air. These minimum creep rates increase with increasing applied stresses, according to a power-law relationship. The minimum creep rate, $\dot{\varepsilon}$, is related to the applied stress, σ, by the following relationship:[19]

$$\dot{\varepsilon} = A\sigma^n \exp\left(-\frac{Q}{RT}\right), \tag{2}$$

where n is the stress exponent, A is a material constant, T is the absolute temperature, Q is the activation energy for creep and R is the gas constant. Fig. 3(a) illustrates that the stress exponent of the Al_2O_3/YAG system decreases with increasing temperatures (from $n = 11.6$ at 1673 K to $n = 9.5$ at 1723 K, $n = 9.2$ at 1773 K, $n = 8.0$ at 1873 K in Al_2O_3/YAG). The Al_2O_3/GAP system with $n = 6.4$ at 1773 K exhibits a slight increase in creep rate by about twice that of Al_2O_3/YAG system at lower stresses of 100–130 MPa and an equivalent in creep rate to Al_2O_3/YAG system at higher stresses of 150–180 MPa, corresponding to results from different melting points (2103 K in Al_2O_3/YAG, 2033 K in Al_2O_3/GAP). Fig. 4(b) shows minimum creep rate as a function of inverse temperature for Al_2O_3/YAG and Al_2O_3/GAP systems in air. Apparent activation energies for creep deformation were obtained from the slope of semi-logarithmic Arrhenius plots of creep rate vs. inverse temperature. Activation energies of the Al_2O_3/YAG system are 737–984 kJ/mol (on average; 864 ± 127 kJ/mol) over the stress range 130–200 MPa. The value of the Al_2O_3/GAP system is 957 kJ/mol at the stress of 150 MPa, which is slightly larger than those of Al_2O_3/YAG system.

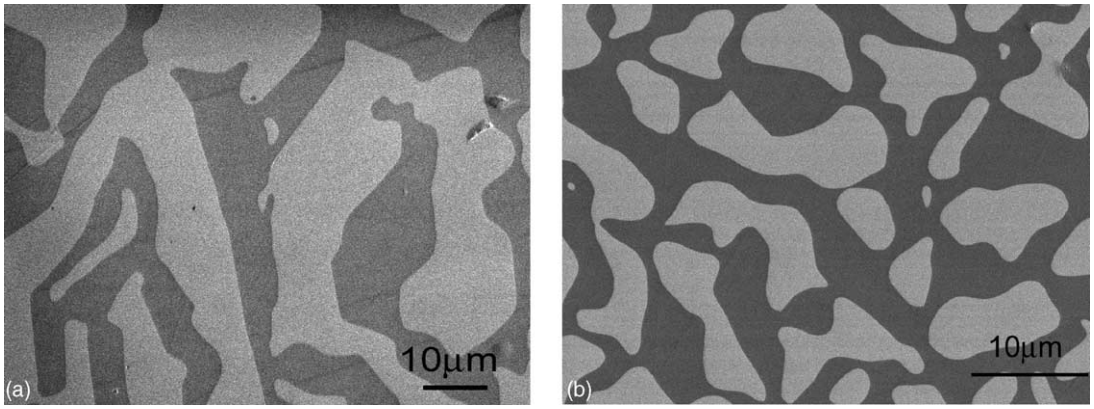

Fig. 2. Scanning electron micrograph of the cross-section parallel to the solidified direction of (a) Al_2O_3/YAG and (b) Al_2O_3/GAP systems at as-received conditions. The dark area is the Al_2O_3 phase and the bright area is the YAG or GAP phase.

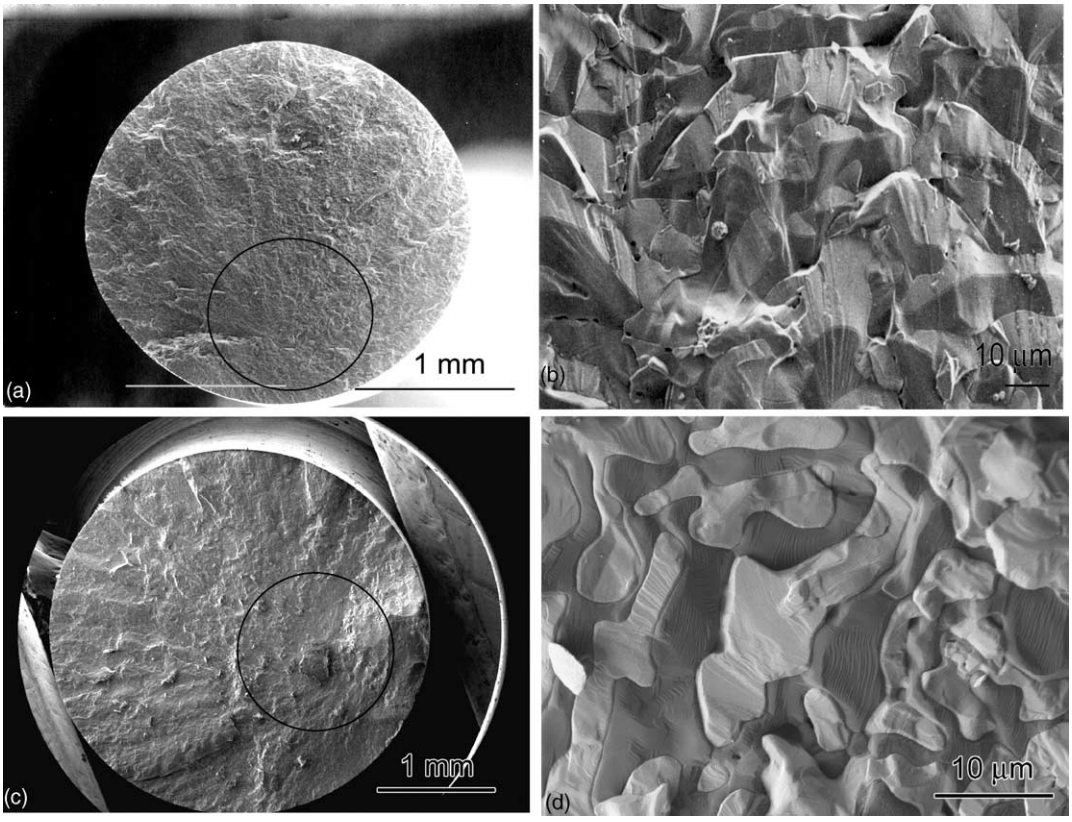

Fig. 3. SEM images of the fracture surface for Al_2O_3/YAG and Al_2O_3/GAP systems after creep at 1773 K and a water vapor pressure of 0.06 MPa. (a) and (c) indicate crack initiation in the specimen interior, which is marked with a circle. (b) and (d) indicate brittle fracture of quasi-cleavage.

3.3. Creep behavior in moisture

Fig. 5(a) shows stress dependence of minimum creep rate for Al_2O_3/YAG and Al_2O_3/GAP systems at 1673–1773 K and a water vapor pressure p_{H_2O} = 0.06 MPa. For comparison creep deformation data in air from Fig. 4(a) is included in Fig. 5(a). In both systems, at a given stress over the temperature of 1673–1773 K, minimum creep rates are larger than those data in air, showing the great difference of creep rates between in air and in moisture at p_{H_2O} = 0.06 MPa at

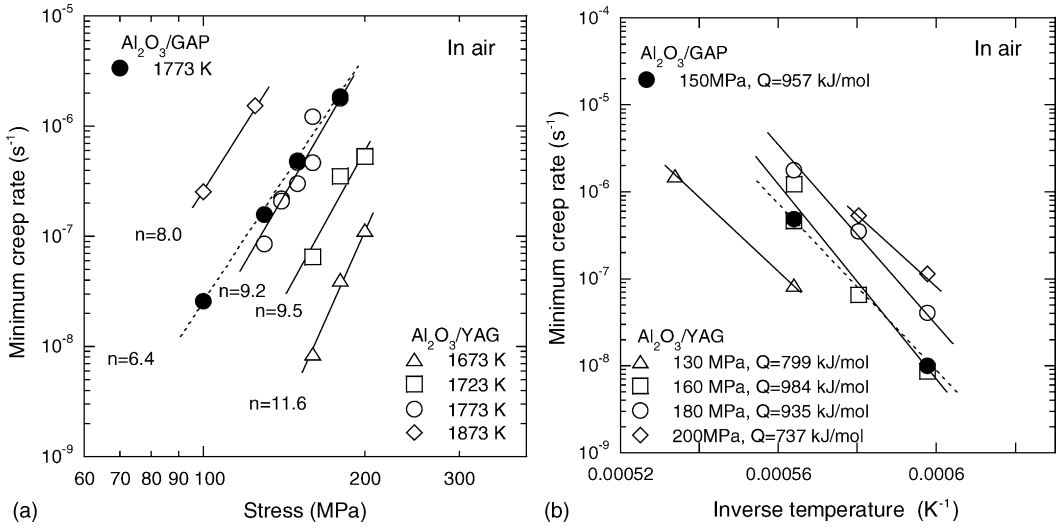

Fig. 4. (a) Minimum creep rate as a function of stress for Al_2O_3/YAG and Al_2O_3/GAP systems at 1673–1873 K in air. In the figure, stress exponents indicate. (b) Minimum creep rate as a function of inverse temperature for Al_2O_3/YAG and Al_2O_3/GAP systems in air. In the figure, activation energies for creep deformation indicate.

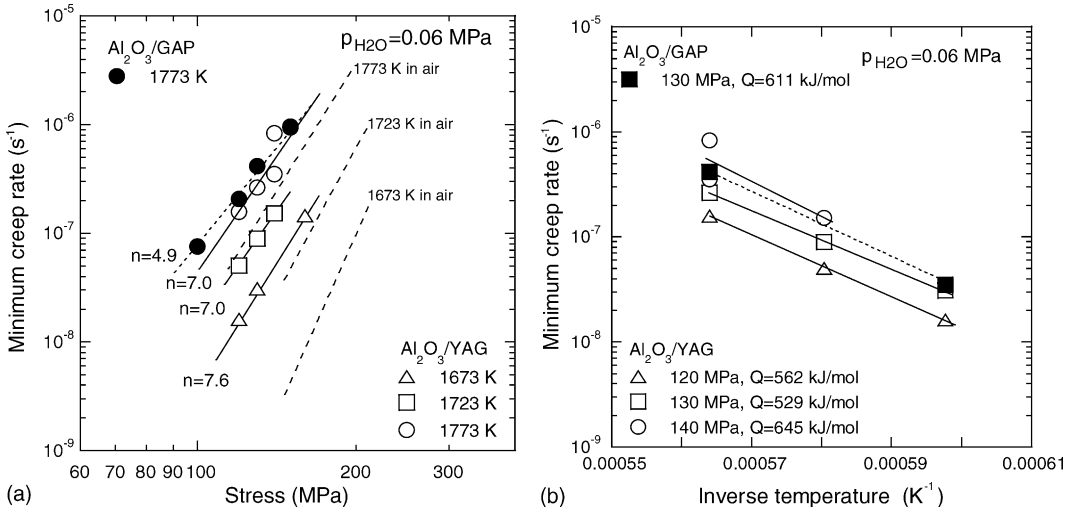

Fig. 5. (a) Minimum creep rate as a function of stress for Al_2O_3/YAG and Al_2O_3/GAP systems at 1673–1773 K and a water vapor pressure of 0.06 MPa. The broken line shows creep data in air. In the figure, stress exponents indicate. (b) Minimum creep rate as a function of inverse temperature for Al_2O_3/YAG and Al_2O_3/GAP systems at a water vapor pressure of 0.06 MPa. In the figure, activation energies for creep deformation indicate.

lower temperatures of 1673–1723 K. The stress exponent varies between 7.0 and 7.6 in the Al_2O_3/YAG system. The Al_2O_3/GAP system with $n = 4.9$ at 1773 K exhibits a slight increase in creep rate by about 0.5–2 that of Al_2O_3/YAG system at lower stresses of 100–130 MPa and an equivalent in creep rate to it at a higher stress of 180 MPa. Fig. 5(b) shows minimum creep rate as a function of inverse temperature for Al_2O_3/YAG and Al_2O_3/GAP systems at $p_{H_2O} = 0.06$ MPa. The slopes of plots of the Al_2O_3/YAG system show activation energies of 529–645 kJ/mol over the stress range 120–140 MPa. The average value is about 579 ± 66 kJ/mol, which is about 285 kJ/mol smaller than that in air. The value of the Al_2O_3/GAP system is 611 kJ/mol at the stress of 130 MPa.

Fig. 6(a) shows stress dependence of minimum creep rate for the Al_2O_3/YAG system at 1673–1773 K and $p_{H_2O} = 0.6$ MPa, together with creep deformation data in air from Fig. 4(a). At a given stress, over the temperature 1673–1773 K, the creep data at $p_{H_2O} = 0.6$ MPa indicates a much larger creep rate than that in air and is slightly larger than that at $p_{H_2O} = 0.06$ MPa. At lower temperature ranges, there was much deference of creep rate between in air and in moisture at $p_{H_2O} = 0.6$ MPa as well as the comparison creep data at $p_{H_2O} = 0.06$ MPa with that in air. The stress exponent is about 6.0–7.0, which is the same, within experimental error, as that at $p_{H_2O} = 0.06$ MPa. Fig. 6(b) shows minimum creep rate as a function of inverse temperature for the Al_2O_3/YAG system at $p_{H_2O} = 0.6$ MPa. Apparent activation energies

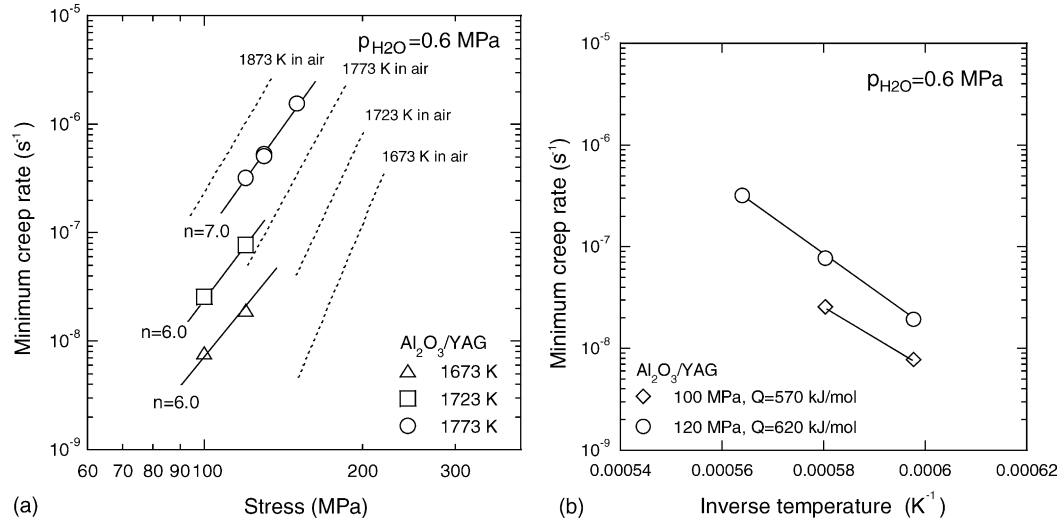

Fig. 6. (a) Minimum creep rate as a function of stress for the Al_2O_3/YAG system at 1673–1773 K and a water vapor pressure of 0.6 MPa. The broken line shows creep data in air. In the figure, stress exponents indicate. (b) Minimum creep rate as a function of inverse temperature for the Al_2O_3/YAG system at a water vapor pressure of 0.6 MPa. In the figure, activation energies for creep deformation indicate.

Table 1
Experimental activation energies for creep deformation of Al_2O_3/YAG and Al_2O_3/GAP systems

Specimen	Test temperature (K)	Test atmosphere	Activation energy, Q (kJ/mol)						
			Applied stress	100 MPa	120 MPa	130 MPa	140 MPa	150 MPa	160 MPa
Al_2O_3/YAG system	1673–1873	Air		–	–	799	–	–	984
	1673–1773	p_{H_2O} = 0.06 MPa		–	562	529	645	–	–
	1673–1773	p_{H_2O} = 0.6 MPa		570	620	–	–	–	–
Al_2O_3/GAP system	1673–1773	Air		–	–	–	–	957	–
	1673–1773	p_{H_2O} = 0.06 MPa		–	–	–	–	611	–

for creep are 570–620 kJ/mol. The average value is about 595 ± 25 kJ/mol, which is close to that at p_{H_2O} = 0.06 MPa, but is about 269 kJ/mol smaller than that in air. Table 1 summarizes activation energies for creep deformation of Al_2O_3/YAG and Al_2O_3/GAP systems obtained in this work.

3.4. Moisture absorption during creep deformation

Typical infrared absorption spectra measured at room temperature are shown in Fig. 7 for the Al_2O_3/YAG system after creep at 1773 K; (A) σ = 140 MPa for 12 h in air, (B) σ = 140 MPa for 18 h in moisture at p_{H_2O} = 0.06 MPa, (C) σ = 150 MPa for 38 h at p_{H_2O} = 0.6 MPa; (D) after exposure at 1773 K for 38 h at p_{H_2O} = 0.6 MPa and (E) for 200 h at p_{H_2O} = 0.6 MPa. All spectra are normalized to a 1 cm optical-path length, so that absorbance of different samples with varying thicknesses could be compared directly. The type of hydroxyl absorption consists of a broad, isotropic band at 3400 cm^{-1} that may extend over 3600–3050 cm^{-1}. Most of the hydroxyl related to molecular water was found in this region of broad band absorption that includes grain, resembling more closely hydroxyl bands of hydrothermally grown sapphire.[18] This type of hydroxyl in the present investigation is the result of molecular water. Hydroxyl concentrations were calculated from Eq. (1), as shown in Table 2. For exposure specimens at 1773 K and at p_{H_2O} = 0.6 MPa, hydroxyl concentrations are very low (about 0.52 ppm for 38 h and 2.14 ppm for 200 h). Creep deformed specimens in both air and moist environments exhibit increased absorption bands caused by hydrogen impurities related to molecular water. This is marked in comparison to an exposure specimen at p_{H_2O} = 0.6 MPa, for which hydroxyl concentrations associated with broad band absorptions are about 5 ppm in air, 8 ppm at p_{H_2O} = 0.06 MPa and 10 ppm at p_{H_2O} = 0.6 MPa, depending on water vapor pressure. These concentrations are less than those for hydrothermally grown sapphire (750 ppm), and hydrothermally annealed and deformed sapphire specimen (25–80 ppm; T = 1173 K and p_{H_2O} = 1500 MPa annealed for 83 h and then 6.9% deformed at 973 K) reported by Kronenberg et al. (Table 3).[18]

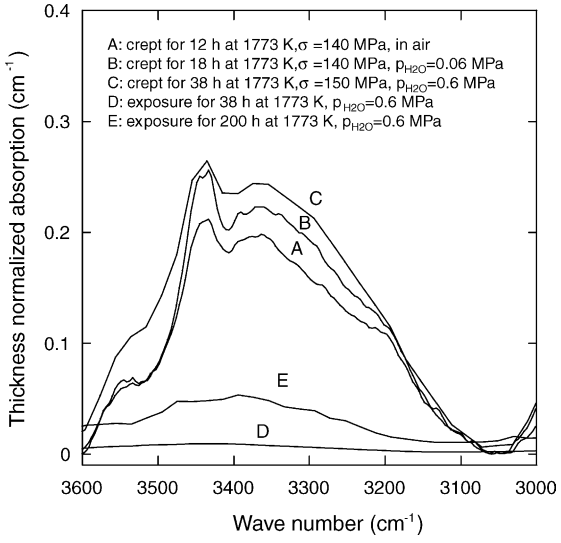

Fig. 7. Infrared absorption spectra for the Al_2O_3/YAG system after creep or exposure specimen at 1773 K in air and moist environments. These spectra represent creep at 1773 K and σ = 140 MPa for 12 h in air (A), for 18 h in moisture at p_{H_2O} = 0.06 (B), σ = 150 MPa for 38 h at p_{H_2O} = 0.6 MPa (C), and exposure at 1773 K for 38 h at p_{H_2O} = 0.6 MPa (D) and for 200 h (E).

3.5. Dislocation structures

Fig. 8 shows bright-filed TEM images of the Al_2O_3/YAG system after creep at 1773 K in air and at p_{H_2O} = 0.06, 0.6 MPa. In Fig. 8(a) and (b) subjected to creep at a strain of about 2.5 % and a stress of 140 MPa in air show that the high dislocation structure is observed in the Al_2O_3 and the YAG phases. Recovery occurs mainly by dislocation climb as evidences by subgrain boundaries. This microstructure indicates that the creep deformation occurs by climb-accommodated dislocation motion. Fig. 8(c)–(f) subjected to creep in moisture at p_{H_2O} = 0.06 MPa (a strain of about 2.5% and a stress of 140 MPa) and 0.6 MPa (a strain of about 2.5% and a stress of 150 MPa), indicate high dislocation structure in both phases as well as in air. The Al_2O_3 phase exhibits that abundant evidence of dislocation motion compared with that of the specimen tested in air. Moderately increased dislocation motion is observed in the YAG phase. However, no recrystallized grains or subgrain boundaries are observed, indicating that recovery is limited.

4. Discussion

Figs. 4–6 indicate that significant differences can be observed when comparing the creep behavior in air and to that

Table 2
Hydroxyl concentration in the Al_2O_3/YAG system and single-crystal alumina examined by IR absorption

Treatment: temperature, duration, environment	Type of OH	Atomic concentration, 10^{-6}OH/Al (ppm)	References
1773 K, 38 h, p_{H_2O} = 0.6 MPa	Broad	0.52	This work
1773 K, 200 h, p_{H_2O} = 0.6 MPa	Broad	2.14	This work
1773 K, 12 h, creep at σ = 140 MPa, air	Broad	4.86	This work
1773 K, 18 h, creep at σ = 140 MPa, p_{H_2O} = 0.06 MPa	Broad	7.84	This work
1773 K, 33 h, creep at σ = 150 MPa, p_{H_2O} = 0.6 MPa	Broad	10.4	This work
Dry seed	Sharp	<0.9	Kronenberg[18]
Hydrothermal growth	Broad	750	Kronenberg[18]
1173 K, 83 h, p_{H_2O} = 1500 MPa; 6.9% deformed at 973 K	Broad	25–80	Kronenberg[18]

Concentrations are indicated in ppm (OH per 10^6 Al ions).

Table 3
Experimental creep data for Al_2O_3/YAG and Al_2O_3/GAP systems in this work

Specimen	Test temperature, T (K)	Applied stress, σ (MPa)	Method	Test atmosphere	Stress exponent, n	Activation energy, Q (kJ/mol)
Al_2O_3/YAG system	1673–1873	100–200	CLT	Air	8.0–11.6	799–984
	1673–1773	120–160	CLT	p_{H_2O} = 0.06 MPa	7.0–7.6	529–645
	1773	100–140	CLT	p_{H_2O} = 0.4 MPa	7.2	–
	1673–1773	100–150	CLT	p_{H_2O} = 0.6 MPa	6.0–7.0	570–620
Al_2O_3/GAP system	1673–1773	100–180	CLT	Air	6.4	957
	1673–1773	100–150	CLT	p_{H_2O} = 0.06 MPa	4.9	611

CLT: constant load tension.

in moisture. Fig. 9 shows a direct comparison of creep behavior in air and moisture at 1773 K for the Al_2O_3/YAG system. Compared to that in air at a given stress, the minimum creep rate in moist environments is higher by about 1.4–4 orders of magnitude for p_{H_2O} = 0.06 MPa, about 5 orders of magnitude for p_{H_2O} = 0.4 MPa, and about 5–7 orders of magnitude for p_{H_2O} = 0.6 MPa. Creep resistance decreases with increasing water vapor pressure up to 0.6 MPa. The stress exponent is approximately 6.0–7.2 (n = 6 at p_{H_2O} = 0.6 MPa, n = 7.2 at p_{H_2O} = 0.06 MPa, and p_{H_2O} = 0.4 MPa); it decreases slightly with increasing water vapor pressure. Data taken from Fig. 9 at a given differential stress are plotted on log–log axes in Fig. 10 to quantify dependence of minimum creep rate on water vapor pressure. Here, the water vapor pressure in air is defined as p_{H_2O} = 0.03 MPa. Therefore, the simple formulation as shown by Norton Eq. (2), cannot be used to analyze

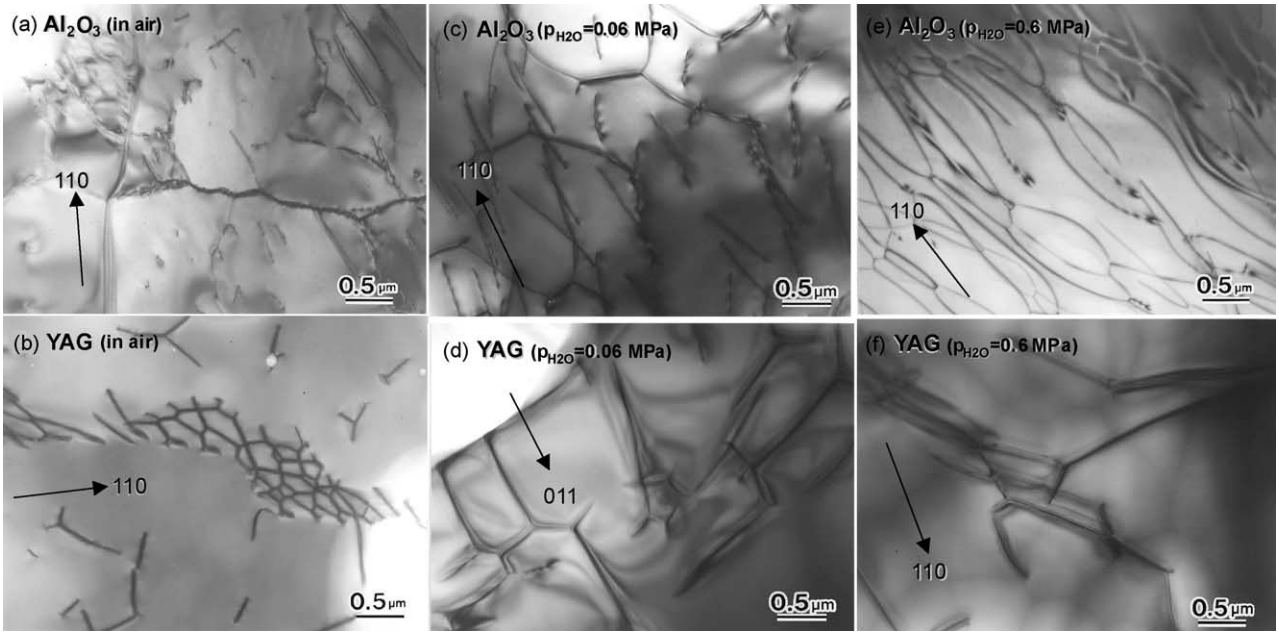

Fig. 8. Bright-field TEM images showing dislocation structures of Al_2O_3 phase and YAG phase after creep at 1773 K in air and in moistures at p_{H_2O} = 0.06, 0.6 MPa.

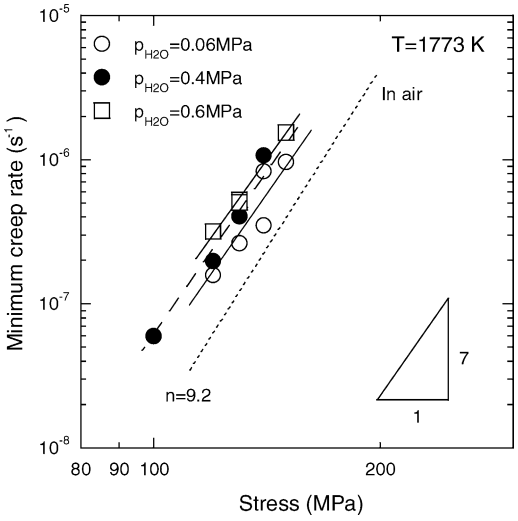

Fig. 9. Minimum creep rate as a function of stress and environments at 1773 K for the Al_2O_3/YAG system.

creep data for the Al_2O_3/YAG system in moisture. This behavior suggests that more than a single factor affects the water vapor pressure dependence of minimum creep rate; one needs at least two parameters to characterize it. The rate of plastic deformation of silicates such as olivine aggregates[20] in a water-rich ("wet") environment can be described as:

$$\dot{\varepsilon} = A_w(p_{H2O})^r \sigma^n \exp\left(-\frac{Q_w}{RT}\right), \quad (3)$$

where A_w is a material constant, r is a constant and, in general, the activation energy (Q_w) can differ from that in air. In our experiment, an average, r, of the result is 0.50 ($r = 0.41$–0.60) at 1773 K over the stress range of 120–150 MPa. Therefore, as creep data for Al_2O_3/YAG system can be followed by Eq. (3), the acceleration of creep rate results from increased water vapor pressure rather than from moisture-induced change in the activation energy for creep ($Q_w = 586 \pm 59$ kJ/mol independent of water vapor pressure).

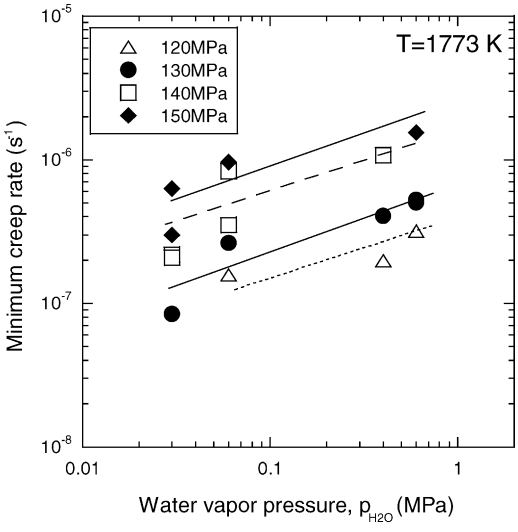

Fig. 10. Minimum creep rate as a function of water vapor pressure for the Al_2O_3/YAG system at 1773 K and stress levels of 120–150 MPa.

It is known that water weakening is a mechanical plastic-weakening effect in the presence of moisture. Previous research on nickel alloys in water environments showed the environmentally enhanced creep behavior during steady-state creep which attributed to a mechanism involving dislocation contraction based on the hydrogen-enhanced localized plasticity model.[21,22] This reasoning is supported by corrosion stresses that revealed lower internal stresses and activation areas in water than in argon, but is not definitively supported in this work for directionally solidified oxide eutectic ceramics. Such an effect has been observed by Castaing et al. on sapphire deformed in a Griggs apparatus.[11,18] Molecular water defects in deformed sapphire were detected only near specimen surfaces, could be introduced in the bulk by diffusion processes and then enhanced dislocation mobility. Castaing et al.[11] attributed the weakening effect to enhanced dislocation glide. The weakening effect in quartz has been attributed to enhanced dislocation glide,[23] or climb[24] due to a chemical action on dislocation velocity in quartz. Similar mechanisms of water incorporation may have been important in the creep acceleration experiments on directionally solidified oxide eutectic ceramics. An alternative explanation can be based on the interaction of the Peierls potential in controlling dislocations and the influence of interstitial hydrogen, which penetrates deep into specimen. Protons from hydrogen or moisture dissolve in sapphire as proton bonded to oxygen ions to form substitutional hydroxide.[25] In general, at high temperature, ionic diffusion becomes fast enough that the propagation of dislocations involves a significant contribution from climb, a diffusion-controlled process. A climb-controlled model has been proposed to explain most high temperature deformation results for directionally solidified oxide eutectic ceramics as well as other ceramics.

5. Conclusion

Environmental effects on ultra-high temperature tensile creep behavior of directionally solidified Al_2O_3/YAG and Al_2O_3/GAP eutectic ceramics was studied using an ultra-high temperature materials testing system simulating severe environments: ultra-high temperatures of 1673–1873 K, stresses from 100–200 MPa, and in air and moist environments at different water vapor pressures ranging up to 0.6 MPa. The directionally solidified oxide eutectic ceramic was followed by the power-law relationship between minimum creep rates and applied stresses. In air, the stress exponent was $n = 6.4$–11.6. The apparent activation energy for creep deformation was Q = 737–984 kJ/mol. While, the presence of moisture led to changes of creep properties. The stress exponent was $n = 4.9$–7.6. The activation energy was approximately 529–645 kJ/mol at $p_{H_2O} = 0.06$ MPa and $Q = 570$–620 kJ/mol at $p_{H_2O} = 0.6$ MPa, independently of

water vapor pressure. The minimum creep rate accelerated by about 1.4–4 orders of magnitude for $p_{H_2O} = 0.06$ MPa, about five orders of magnitude for $p_{H_2O} = 0.4$ MPa and about 5–7 orders of magnitude for $p_{H_2O} = 0.6$ MPa as compared to that in air at 1773 K. Creep deformed specimens in both air and moist environments exhibited increased hydrogen impurities related to molecular water. The microstructure indicated that creep deformation occurred by dislocation motion, showing abundant evidence of dislocation motion in the Al_2O_3 phase and moderate motion in the YAG phase. Results of this study and reasonable estimates in changes of the water vapor pressure indicated accelerated creep behavior by the presence of moisture.

Acknowledgements

This research was supported by Industrial Technology Research Grant Program in 2001 from New Energy and Industrial Technology Development Organization (NEDO) of Japan. We also acknowledge Dr. S. Sakata (Ube Co. Ltd.) for preparing test samples and Sumitomo Metals Technology Inc. for TEM and FTIR test.

References

1. Waku, Y., Nakagawa, N., Ohtsubo, H., Ohsora, Y. and Kohtoku, Y., High temperature properties of unidirectionally solidified Al_2O_3-YAG composites. *J. Jpn. Inst. Metals*, 1995, **59**, 71–78.
2. Waku, Y. and Sakuma, T., Dislocation mechanism of deformation and strength of Al_2O_3-YAG single crystal composites at high temperatures above 1500 °C. *J. Eur. Ceram. Soc.*, 2000, **20**, 1453–1458.
3. Waku, Y., Nakagawa, N., Wakamoto, T., Ohtsubo, H., Shimizu, K. and Kohtoku, Y., The creep and thermal stability characteristics of a unidirectionally solidified Al_2O_3/YAG eutectic composite. *J. Mater. Sci.*, 1998, **33**, 4943–4951.
4. Waku, Y., High temperature characteristics of melt growth composites with a novel microstructure. *J. Jpn. Inst. Metals*, 2000, **64**, 977–984.
5. Waku, Y., High temperature properties and thermal stability of a unidirectionally solidified $Al_2O_3/Er_3Al_5O_{12}$ eutectic composite. *J. Jpn. Inst. Metals*, 2000, **64**, 101–107.
6. Waku, Y., Sakata, S., Mitani, A. and Shimizu, K., High-temperature strength and a microstructure of an $Al_2O_3/Er_3Al_5O_{12}/ZrO_2$ ternary MGC. *J. Jpn. Inst. Metals*, 2000, **64**, 1263–1268.
7. Troiano, A. R., The role of hydrogen and other interstitials on the mechanical behavior of metals. *Trans. ASM*, 1960, **52**, 54–80.
8. Fowler Jr., J. D., Causey, R. A., Chandra, D., Elleman, T. S. and Verghese, K., Tritium diffusion in ceramic materials for thermonuclear reactors. *J. Vac. Sci. Technol.*, 1976, **13**, 401–402.
9. Tai, W. P., Watanabe, T. and Jacobson, N. S., High-temperature stability of alumina in argon and argon/water-vapor environments. *J. Am. Ceram. Soc.*, 1999, **82**, 245–248.
10. Kronenberg, A. K., Kirby, S. H., Aines, R. D. and Rossman, G. R., Solubility and diffusional uptake of hydrogen in quartz at high water pressures-implications for hydrolytic weakening. *J. Geophys. Res.*, 1986, **91**, 2723–2744.
11. Castaing, J., Kronenberg, A. K., Kirby, S. H. and Mitchell, T. E., Hydrogen defects in α-Al_2O_3 and water weakening of sapphire and alumina ceramics between 600 and 1000 °C-II. Mechanical Properties. *Acta Mater.*, 2000, **48**, 1495–1504.
12. Pollock, J. T. A. and Hurley, G. F., Dependence of room temperature fracture strength on strain-rate in sapphire. *J. Mater. Sci.*, 1973, **8**, 1595–1602.
13. Sayir, A., Time-dependent strength of sapphire fibers at high temperatures. In *Advances in Ceramic-Matrix Composites II*, ed. J. P. Singh and L. P. Bansal. The American Ceramic Society, Westerville, OH, 1994, pp. 691–702.
14. Heuer, A. H., Firestone, R. F., Snow, J. D. and Tullis, J., In *Ceramics in Severe Environments*, ed. W. W. Kriegel and H. Palmour III. Plenum Press, New York, 1971, pp. 331–340.
15. Kronenberg, A. K., SILICA physical behavior geochemistry and materials applications. In *Reviews in Mineralogy*, *29*, ed. P. J. Heaney, C. T. Prewitt and G. V. Gibbs. 1994, p. 123.
16. Harada, Y., Suzuki, T., Hirano, K. and Waku, Y., Influence of moisture on ultra-high temperature tensile creep behavior of in-situ single-crystal oxide ceramic Al2O3/YAG eutectic composite. *J. Am. Ceram. Soc.*, 2003, **86**, 951–958.
17. Harada, Y., Suzuki, T., Hirano, K. and Waku, Y., Moisture acceleration of tensile creep behavior in in-situ single-crystal oxide ceramic eutectic composites. In *Proceedings of the 10th International Ceramics Congress-Part C*, ed. P. Vincenzini. Techna S.r.l., Faenza, 2003, pp. 815–822.
18. Kronenberg, A. K., Castaing, J., Mitchell, T. E. and Kirby, S. H., Hydrogen defects in α-Al_2O_3 and water weakening of sapphire and alumina ceramics between 600 and 1000 °C-I. Infrared characterization of defects. *Acta Mater.*, 2000, **48**, 1481–1494.
19. Frost, H. J. and Ashby, M. F., *Deformation Mechanism Maps: The Plasticity and Creep of Metals and Ceramics*. Pergamon Press, Oxford, 1982.
20. Mei, S. and Kohlstedt, D. L., Influence of water on plastic deformation of olivine aggregates: 2. dislocation creep regime. *J. Geophys. Res.*, 2000, **91**, 21471–21481.
21. Angeliu, T. M., Paraventi, D. J. and Was, G. S., Creep and interglanular cracking behavior of nickel-chromium-iron-carbon alloys in 360 °C water. *Corrosion*, 1995, **51**, 837–848.
22. Paraventi, D. J., Angeliu, T. M. and Was, G. S., Effect of hydrogen on creep in high-purity Ni-16Cr-9Fe alloys at 360 °C. *Corrosion*, 2002, **58**, 675–686.
23. Griggs, D. T., A model of water weakening in quartz. *J. Geophys. Res.*, 1974, **14**, 19–31.
24. Post, A. and Tullis, J., The rate of water penetration in experimentally deformed quartzite: implications for hydrolytic weakening. *Tectonophysics*, 1998, **295**, 117–137.
25. Norby, T., Protonic defects in oxides and their possible role in high temperature oxidation. *J. de Phys. IV*, 1993, **3**, 99–106.